Application of operator-scaling anisotropic random fields to binary mixtures

Denis Anders, Alexander Hoffmann, Hans-Peter Scheffler, Kerstin Weinberg

Application of operator-scaling anisotropic random fields to binary mixtures

Journal:	*Philosophical Magazine & Philosophical Magazine Letters*
Manuscript ID:	TPHM-11-Feb-0053.R1
Journal Selection:	Philosophical Magazine
Date Submitted by the Author:	09-May-2011
Complete List of Authors:	Anders, Denis; University of Siegen Hoffmann, Alexander; University of Siegen, Chair of Probability Theory and Analysis Scheffler, Hans-Peter; University of Siegen, Chair of Probability Theory and Analysis Weinberg, Kerstin; University of Siegen, Chair of Solid Mechanics
Keywords:	mechanics of materials, phase decomposition, microstructure
Keywords (user supplied):	random fields

Philosophical Magazine
Vol. 00, No. 00, 00 Month 2011, 1–27

RESEARCH ARTICLE

Application of operator-scaling anisotropic random fields to binary mixtures

Denis Anders[a]*, Alexander Hoffmann[b], Hans-Peter Scheffler[b] and Kerstin Weinberg[a]

[a] *Chair of Solid Mechanics, University of Siegen, Paul-Bonatz-Straße 9-11, 57068 Siegen, Germany*; [b] *Chair of Probability Theory and Analysis, University of Siegen, Walter-Flex-Straße 3, 57068 Siegen, Germany*

(*Received 00 Month 200x; final version received 00 Month 200x*)

In modern technical applications various multiphase mixtures are used to meet demanding mechanical, chemical and electrical requirements. To understand their structural properties as continuous macroscopic materials, it is important to capture the microstructure of these mixtures. Due to their vast range of applications multicomponent systems are subjected to microstructural changes as phase separation and coarsening. Therefore the ultimate microstructural arrangement depends on the system's configuration and on exterior driving forces. In addition to this, random physical imperfections within the material and random noises in the exterior thermodynamic fields influence in essence the microstructural evolution. Since all physical processes are subjected to a certain degree of random inhomogeneity under realistic conditions, the influence of random phenomena cannot be neglected in modern physical models. An advanced mathematical description and an implementation of these stochastic processes are required to adapt simulation results basing on deterministic mathematical models to experimental observations. In our contribution we will present an operator-scaling anisotropic random field embedded in the Cahn-Hilliard phase-field model to describe the phase evolution in a binary mixture. The arising non-linear diffusion equation will be solved numerically in the innovative framework of isogeometric finite element method. To illustrate the flexibility and versatility of our approach, numerical and experimental results for an eutectic Sn-Pb alloy are contraposed. It is the first time that the microstructural evolution in a multicomponent system is associated with operator-scaling anisotropic random fields. Due to its enormous potential as an essential ingredient in stochastic mathematical and physical modeling it is only a matter of time until these processes will become prevalent in engineering applications.

Keywords: binary alloys, solder, spinodal decomposition, phase-field, random fields

1. Introduction

Until recently, material modeling and studies on microstructure have mainly been subjects to empirical sciences. Systematic experimental observations provided the key to derive constitutive and structural properties of the considered materials. However, in the last decades mathematical modeling of materials on different length- and timescales have become a matter of great scientific interest. Now the main objective is to develop a model and to perform numerical simulations in order to gain understanding of physical processes within the material. Furthermore, such models should yield indications to predict the material behavior for future applications. At this, experimental data are still an essential source for the validation and parametrization of the educed material model. Any modeler aspires to implement a minimal set of parameters to match the model with experiments. Here it is crucial to figure out dominant effects, driving quantities of secondary order and variables,

*Corresponding author. Email: anders@imr.mb.uni-siegen.de

ISSN: xxxx-xxxx print/ISSN xxxx-xxxx online

DOI: 10.1080/14786435.20xx.xxxxxx
http://www.informaworld.com

which are negligible. The goal is always to derive a rather simple model but to approximate adequately complex processes in reality.
The fast development in the area of scientific computing gives rise to embedding the mathematical material models into the framework of a numerical approximation scheme, such as e.g. spectral methods [11, 31] or finite element analysis [51]. However, many of the numerical results clearly reflect the simplifications of the underlying model. In particular, in the field of diffusion induced phase separation and coarsening the computed processes do correctly map the separation of the mixture into different phases and also, e.g., the rate of phase growth, [32, 47]. However, the computed microstructure of circular phase islands or ideally smooth lamellae is not realistic. A typical microstructure observed during experimental investigations of phase evolution in an eutectic Sn-Pb solder is shown in Figure 1. The micrograph shows areas of different microstructural arrangements at the same instance of time. There are some domains where oriented lamellae-like structures evolve and, in neighboring regions, contorted bubble-like particles emerge. In general, it is extremely cumbersome to derive a theory that is able to capture the great variety of real life observations in experimental studies of microstructure. The reasons for deviations between experiments and *idealized* theories may be found in the general imperfection of nature where always perturbations, e.g. temperature fluctuations and inhomogeneities during solidification, occur. However, the specific microstructure is directly affected by physical imperfections within the material and by random deviations in the exterior thermodynamic fields, such as thermal and mechanical loads. In our opinion, the influence of such random phenomena cannot be neglected in modern physical models.

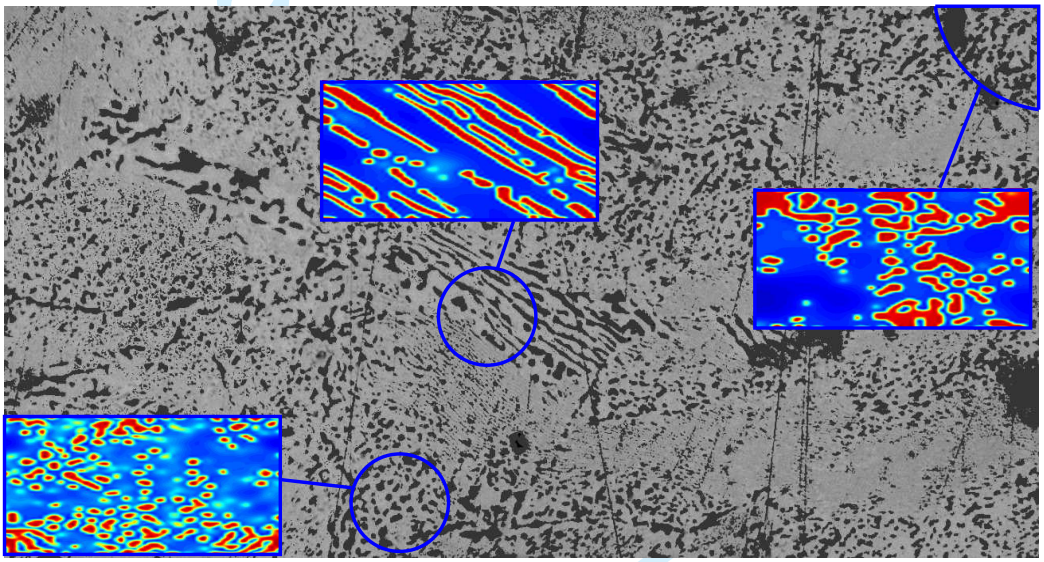

Figure 1.: Optical micrograph of a $100\,\mu\text{m} \times 50\,\mu\text{m}$ eutectic Sn-Pb solder after 10h of aging at an operating temperature of 420 K. The bluish images denote the corresponding simulated microstructure.

With the aim to account for such perturbations we present here a new approach to describe microstructural phase evolution. To this end we introduce a coherent diffusion model for spinodal decomposition and continuous ordering subjected to fluctuating driving forces. In order to map random fluctuations we make use of an operator-scaling anisotropic random field and embed it in the Cahn-Hilliard phase-field model to describe the phase evolution in a binary mixture. Although a similar technique has been employed, e.g. for superdiffusive spreading of passive

scalars in turbulent and chaotic flow and for flow through porous media [9, 50], it is the first time that the microstructural evolution in a multicomponent system is associated with operator-scaling anisotropic random fields. By now this new class of random fields has been receipted only among mathematicians. However, due to its enormous potential as an essential ingredient in stochastic physical modeling, it is only a matter of time until operator-scaling random fields will become prevalent in engineering applications.

The interest in randomly forced diffusion phenomena goes back to the very early works of Cahn, Cook and Hilliard [19]. Since all subsequent models base on this theory, we provide in Section 2 of this paper a concise synopsis of the Cahn-Hilliard-Cook diffusion model. A critical review of the stochastic model concludes this section. Section 3 is entirely devoted to a short overview of operator-scaling anisotropic random fields and the functionality of the control variables employed in our specific random field. In Section 4 we include a fluctuating driving force in the deterministic diffusion equation and deduce the variational formulation of the considered problem. Numerical experiments in Section 5 demonstrate the versatility and flexibility of our approach. A contrasting comparison of our results and a concise summary in Section 6 will conclude this manuscript.

2. Stochastic diffusion models

In this section we elaborate on the state of the art of stochastic diffusion models for spinodal decomposition and phase coarsening. The deterministic model for spinodal decomposition in alloys goes back to the early research work of Cahn and Hilliard in the 1960s [12–16]. Although this model is able to depict the predominant driving quantities such as minimization of thermodynamic free energy and surface energy, it still lacks a complete description of the diffusion process. Discrepancies between the deterministic Cahn-Hilliard theory and experimental results especially during the very early stages of spinodal decomposition motivated Cook to incorporate an additional random variable into the diffusion model at hand, [19]. His objective was to embed a random flux resulting from thermal fluctuations, i.e., Brownian movement, in the Cahn-Hilliard model according to a mathematically consistent fluctuation theory. At that time Brownian motion was a well understood stochastic process [10, 26, 27, 48], described by the commonly known Langevin equation [41]. Therefore Cook included in his model a random field analogously to the fluctuating force in the Langevin equation. To this end, he had to bring the stochastically extended Cahn-Hilliard equation into a formulation equivalent to a Langevin-type model. Let us now briefly outline the main steps of Cook's derivation in order to point out our criticism on his theory. We start with a formulation of the mass current $\mathbf{j}$ for a binary system

$$\mathbf{j} = -M \nabla \delta_c \Psi, \tag{1}$$

where M denotes the constant Onsager coefficient (mobility) for an isotropic solution and Ψ is the total free energy density of the system namely

$$\Psi(c) = \Psi^{\mathrm{con}}(c) + \frac{\lambda}{2} \|\nabla c\|^2 . \tag{2}$$

Here Ψ^{con} comprises the configurational energy density and the second term involves the surface energy contribution. The $\delta_c(\bullet)$ operator is in the context of Eq. (1) the variational derivative with respect to the concentration field c. Assum-

ing homogeneous Neumann boundary conditions $\nabla c \cdot \mathbf{n} = 0$ as natural boundary conditions it holds $\delta_c(\bullet) = \partial_c(\bullet) - \nabla \cdot \partial_{\nabla c}(\bullet)$. The vector field $\mathbf{n}$ denotes the unit outward normal to the considered domain. Now Cook extends the continuity equation by a quasi-random flux contribution $\tilde{\mathbf{j}}$, that fulfills the mass-conserving boundary condition $\left(\mathbf{j} + \tilde{\mathbf{j}}\right) \cdot \mathbf{n} = 0$. The entire diffusion equation then reads

$$\frac{\partial c(\mathbf{x},t)}{\partial t} = -\nabla \cdot \left(-M \nabla \delta_c \Psi(\mathbf{x},t) + \tilde{\mathbf{j}}(\mathbf{x},t)\right), \text{ with } (\mathbf{x},t) \in \Omega \times [0,\mathcal{T}]. \quad (3)$$

Since Cook was not able to precisely specify $\tilde{\mathbf{j}}$, he introduces a fluctuating scalar field $g(\mathbf{x},t)$ which is related to $\tilde{\mathbf{j}}$ by

$$\tilde{\mathbf{j}} = -\nabla g(\mathbf{x},t). \quad (4)$$

In this manner Cook is able to characterize the average properties of the Fourier transform of $g(\mathbf{x},t)$. Taking Eq. (4) into account and accomplishing a Fourier transform of the continuity equation (3) delivers the desired Langevin-type equation in Fourier space

$$\frac{\partial \hat{c}(\mathbf{k},t)}{\partial t} = \alpha(\mathbf{k})\,\hat{c}(\mathbf{k},t) - \|\mathbf{k}\|^2 \hat{g}(\mathbf{k},t), \quad (5)$$

where $\hat{(\bullet)}$ symbolizes the Fourier transform of the corresponding field, $\mathbf{k}$ is the wave vector and $\alpha(\mathbf{k})$ is an amplification factor given by

$$\alpha(\mathbf{k}) = -\|\mathbf{k}\|^2 M \left(\partial_c^2 \Psi^{\text{con}} + \lambda \|\mathbf{k}\|^2\right). \quad (6)$$

A detailed derivation of the amplification factor may be found in the Appendix. The field $\|\mathbf{k}\|^2 \hat{g}(\mathbf{k},t)$ in Eq. (5) is the counterpart to the random force in the Langevin equation. In the style of Uhlenbeck and Ohrnstein [48] Cook analyzes the intensity expression

$$\mathcal{I}(\mathbf{k},t) = \hat{c}(\mathbf{k},t)\,\overline{\hat{c}(\mathbf{k},t)} \quad (7)$$

to obtain the average properties of $\hat{g}(\mathbf{k},t)$. Cook focusses here on the intensity expression (7) because it is impossible to measure the Fourier amplitudes $\hat{c}$ directly. Instead, the kinetics of spinodal decomposition and continuous ordering can be studied experimentally by the so-called diffraction techniques where an X-ray intensity is measured in the sample, cf. [18, 46].
Since Eq. (5) can be solved analytically by

$$\hat{c}(\mathbf{k},t) = \hat{c}(\mathbf{k},0)\, e^{\alpha(\mathbf{k})t} - \|\mathbf{k}\|^2 e^{\alpha(\mathbf{k})t} \int_0^t e^{-\alpha(\mathbf{k})\zeta} \hat{g}(\mathbf{k},\zeta)\, \mathrm{d}\zeta, \quad (8)$$

the intensity expression becomes

$$\mathcal{I}(\mathbf{k},t) = e^{2\alpha(\mathbf{k})t} \left(\hat{c}(\mathbf{k},0)\,\overline{\hat{c}(\mathbf{k},0)} - \|\mathbf{k}\|^4 \int_0^t \int_0^t e^{-\alpha(\mathbf{k})(\zeta+\zeta')} \left\langle \hat{g}(\mathbf{k},\zeta)\,\overline{\hat{g}(\mathbf{k},\zeta')} \right\rangle \mathrm{d}\zeta \mathrm{d}\zeta'\right). \quad (9)$$

The cross terms in $\hat{c}(\mathbf{k},t)$ and $\hat{g}(\mathbf{k},t)$ do not appear here, because the average value of $\hat{g}(\mathbf{k},t)$ is set to zero. Additionally, Cook assumes that the spectral resolution

of the correlation function $\left\langle \hat{g}\left(\mathbf{k},\zeta\right)\overline{\hat{g}\left(\mathbf{k},\zeta'\right)}\right\rangle$ can be separated into a spatial and a temporal term according to

$$\left\langle \hat{g}\left(\mathbf{k},\zeta\right)\overline{\hat{g}\left(\mathbf{k},\zeta'\right)}\right\rangle = Q\left(\mathbf{k}\right)\delta\left(\zeta-\zeta'\right). \tag{10}$$

The spatial term is then determined from the equilibrium intensity distribution $\mathcal{I}\left(\mathbf{k},t=\infty\right)$ of a stable single-phase solid solution (with $\alpha\left(\mathbf{k}\right)<0$ for all $\mathbf{k}$). Following arguments based on fluctuation theory [39], one obtains the relation

$$\frac{\left\|\mathbf{k}\right\|^4 Q\left(\mathbf{k}\right)}{\alpha\left(\mathbf{k}\right)} = \frac{k_B T}{c_0\left(1-c_0\right)v\left(\partial_c^2\Psi^{\mathrm{con}}+\lambda\left\|\mathbf{k}\right\|^2\right)}, \tag{11}$$

with mean composition c_0, volume per atom v and thermal energy k_BT. For a more detailed derivation of the presented expressions the authors refer to Cook's original work [19, 20]. In recent papers the authors often use a random force ξ with $\xi\left(\mathbf{x},t\right)=\Delta g\left(\mathbf{x},t\right)$ instead of a noisy flux contribution [5, 28, 34, 35]. Analogously, one obtains for $\left\langle \hat{\xi}\left(\mathbf{k},\zeta\right)\overline{\hat{\xi}\left(\mathbf{k},\zeta'\right)}\right\rangle = \mathcal{Q}\left(\mathbf{k}\right)\delta\left(\zeta-\zeta'\right)$ a similar result

$$\frac{\mathcal{Q}\left(\mathbf{k}\right)}{\alpha\left(\mathbf{k}\right)} = \frac{k_B T}{c_0\left(1-c_0\right)v\left(\partial_c^2\Psi^{\mathrm{con}}+\lambda\left\|\mathbf{k}\right\|^2\right)} \tag{12}$$

$$\Leftrightarrow \mathcal{Q}\left(\mathbf{k}\right) = -\frac{\left\|\mathbf{k}\right\|^2 M k_B T}{c_0\left(1-c_0\right)v} = -2\left\|\mathbf{k}\right\|^2 M^* k_B T \tag{13}$$

with a generalized mobility M^*. Remark that Eq. (13) is the spectral resolution of the correlation of ξ according to [42]. Taking the inverse Fourier transform of Eq. (13) and exploiting $\widehat{\left(\delta\left(\mathbf{x}\right)\right)}=1$ leads to the usual correlation expression

$$\left\langle \xi\left(\mathbf{x},t\right)\xi\left(\mathbf{x}',t'\right)\right\rangle = -2M^* k_B T\Delta\delta\left(\mathbf{x}-\mathbf{x}'\right)\delta\left(t-t'\right). \tag{14}$$

In the context of Eq. (14) the laplacian is meant in the distributional sense. Eq. (14) expresses that the fluctuating force ξ is uncorrelated in time and partly correlated in space showing a short-range behavior. So far, all research work on the stochastic Cahn-Hilliard model bases on Gaussian noises with the short-range correlation in Eq. (14). Although Barros et al. proposed in [5]

$$\left\langle \xi\left(\mathbf{x},t\right)\xi\left(\mathbf{x}',t'\right)\right\rangle = M^* k_B T\delta\left(\mathbf{x}-\mathbf{x}'\right)\delta\left(t-t'\right) \tag{15}$$

as a novel form of the noise correlation for a non-conserved order parameter, it still does not exceed the short-range regime.

Numerical studies of the microstructural evolution described by the Cahn-Hilliard-Cook model showed no significant difference compared to the results performed by the deterministic diffusion model. In addition to it, Eq. (4) must be critically reviewed. It is *not* possible to define a reasonable fluctuating scalar field, which is differentiable. The authors regard the limitation to isotropic short-range correlations as an intrinsic shortcoming of the Cahn-Hilliard-Cook theory. Therefore, we suggest to introduce a novel approach to include an anisotropic and long-range stochastic process into the Cahn-Hilliard diffusion model.

3. Operator-scaling anisotropic random fields

In this section we briefly describe time varying operator-scaling random fields and their simulation. These fields are generalizations of the random fields introduced in [9]. For more details and a rigorous mathematical treatment of time varying operator-scaling random fields we refer to [9, 50].

Brownian motion of particles is a simple, non-correlated random motion seen, e.g., in swirling gas molecules. More organized systems, however, tend to continuous-time random walks or Lévy-walks. Figuratively speaking, Lévy walks are a mix of long trajectories and short random movements found, e.g., in turbulent fluids but also in the motion of fish schools, human travel behavior and financial risk theory. A stable Lévy motion is a self-similar process. Recall that a stochastic process $\{X(r)\}_{r\in\mathbb{R}^d}$ taking values in $\mathbb{R}^d$ is self-similar if

$$\{X(cr)\}_{r\in\mathbb{R}^d} \stackrel{d}{=} \{c^H X(r)\}_{r\in\mathbb{R}^d} \quad \text{at every scale } c>0. \tag{16}$$

Symbol $\stackrel{d}{=}$ indicates equality of finite dimensional distributions; and we assume X to be stochastically continuous. The scaling parameter $H>0$ is commonly called the *Hurst index*. Operator-scaling self-similar processes allow the Hurst index to vary with the coordinates. For the specific fields we have in mind here, the operator scales with the x-, y- and t-directions. Following the approach of [9, 22] we define a scalar valued random field $\{X(cr)\}_{r\in\mathbb{R}^d}$ to be operator-scaling if for some $d\times d$ matrix $\bar{\mathbf{E}}$ with positive real parts of the eigenvalues and some $H>0$ we have

$$\{X(c^{\bar{\mathbf{E}}}r)\}_{r\in\mathbb{R}^d} \stackrel{d}{=} \{c^H X(r)\}_{r\in\mathbb{R}^d} \qquad \text{for all } c>0. \tag{17}$$

Here $c^{\bar{\mathbf{E}}}$ is given by $c^{\bar{\mathbf{E}}} = \exp(\bar{\mathbf{E}}\log c)$ where $\exp(\mathbf{A}) = \sum_{k=0}^{\infty}\frac{\mathbf{A}^k}{k!}$ is the matrix exponential. Note that if $\bar{\mathbf{E}}=\mathbf{I}$, the identity matrix, condition (17) is just the self-similarity property (16).

Now, let $W(\mathrm{d}\mathbf{y}\times\mathrm{d}s)$ be a complex-valued independently scattered isotropic random Gaussian measure on $\mathbb{R}^2\times\mathbb{R}$. Roughly speaking, this means that for disjoint sets $\mathcal{A}_1,\mathcal{A}_2\subset\mathbb{R}^3$, $W(\mathcal{A}_1)$ and $W(\mathcal{A}_2)$ are independent isotropic complex-valued normal random variables with mean zero and variance comparable to the volume of $\mathcal{A}_1$ and $\mathcal{A}_2$, respectively. Such random fields can be simulated easily.

Now for $(\mathbf{x},t)\in\Omega\times[0,t_{\max}]\,, t_{\max}\le\mathcal{T}$ and parameters $0<H_1,H_2,H_3<1$ we define a random field by

$$\bar{\xi}(\mathbf{x},t) = \mathrm{Re}\int_{\mathbb{R}^2\times\mathbb{R}}\left(e^{i\mathbf{x}\cdot\mathbf{y}}-1\right)\left(e^{i(t_{\max}-t)s}-1\right)\cdot\psi_1(\mathbf{y})\cdot\psi_2(s)W(\mathrm{d}\mathbf{y}\times\mathrm{d}s), \tag{18}$$

where

$$\psi_1(\mathbf{y}) = \left(|\mathbf{y}\cdot\theta_1|^{2H_1}+|\mathbf{y}\cdot\theta_2|^{2H_2}\right)^{-\frac{H_1+H_2}{4}-\frac{1}{2}} \tag{19}$$

$$\psi_2(s) = \frac{1}{|s|^{\frac{1+2H_3}{2}}}. \tag{20}$$

Here θ_1,θ_2 are normalized eigenvectors of a matrix $\mathbf{E}$ with given eigenvalues H_1^{-1},H_2^{-1}, respectively. Hence the spatial scaling matrix $\mathbf{E}$ is fully determined by 4 parameters. The field (18) is anisotropic if the spatial scaling relation has different Hurst indices in the – not necessarily orthogonal – directions of eigenvectors

θ_1, θ_2. The intensity of the field in the course of time is scaled by H_3.
With respect to mass conservation in a representative domain Ω we need to claim for an appropriate random field

$$\int_\Omega \xi(\mathbf{x}, t)\, \mathrm{d}\mathbf{x} = 0 \quad \forall t \in [0, t_{\max}], \tag{21}$$

which we easily get by the transformation

$$\xi(\mathbf{x}, t) = \bar{\xi}(\mathbf{x}, t) - \frac{1}{|\Omega|} \int_\Omega \bar{\xi}(\mathbf{y}, t)\, \mathrm{d}\mathbf{y} \quad \forall t \in [0, t_{\max}], \tag{22}$$

which is well-defined since the random field $\bar{\xi}$ exists for the given parameters and has continuous sample path. The term $|\Omega|$ denotes the corresponding Lebesgue measure of Ω.
Compared to Gaussian white noise or the Gaussian random fields with covariance structure given by (14) or (15), respectively, our fields are much more flexible. In contrast to the short range dependence of the fields defined by (14) and (15), our random field defined by (18) allows to model long range dependencies in the spatial and temporal coordinates separately. Moreover it can have anisotropic behavior in space. See section 3.1 below. Observe further, that the random field defined by (18) is always *decoupled* in space and time by construction (see (23) and (24) below). There are other types of random fields as in [9] which allow dependencies between space and time scaling. However, from our point of view this seems unrealistic and hence, we restrict our attention to fields defined by (18).

3.1. *Parameter handling and scaling properties*

With our model we are capable of exerting control on the range of dependence in space and time as well as on the anisotropic behavior, according to Eq. (18). In the following we want to show how to control the random field by the given parameters. One can show the following scaling properties:

$$\xi(a^{\mathbf{E}}\mathbf{x}, t) \overset{d}{=} a\xi(\mathbf{x}, t), \tag{23}$$

$$\xi(\mathbf{x}, a^{H_3^{-1}} t) \overset{d}{=} a\xi(\mathbf{x}, t), \tag{24}$$

where d means again equality of all finite-dimensional marginal distributions for the random fields. Hence, by setting the global scaling matrix

$$\bar{\mathbf{E}} := \begin{pmatrix} \mathbf{E}_{2\times 2} & \mathbf{0}_{1\times 2} \\ \mathbf{0}_{2\times 1} & 0 \end{pmatrix} + \begin{pmatrix} \mathbf{0}_{2\times 2} & \mathbf{0}_{1\times 2} \\ \mathbf{0}_{2\times 1} & H_3^{-1} \end{pmatrix} \tag{25}$$

the random field has two *independent* scaling properties, one for the spatial and one for the temporal component. In this context the notation $\mathbf{A}_{i\times j}$ denotes that $\mathbf{A}$ is an $(i \times j)$-matrix.
The presented fundamental property implies a rather flexible simulation model. In space we want to control the degree of anisotropy, its orientation and the range of spatial dependence as shown below. Independent from that feature we would like to control the temporal dependence by the parameter H_3 from short to long range dependence.
The parameters H_1 respectively H_2 can be interpreted as Hurst indices in direction

θ_1 and θ_2 in the following way: For a fixed time $t \in [0, t_{\max}]$ we define for both directions θ_1, θ_2 the subprocess

$$\xi_{\theta_i}(r) := \xi(r\theta_i, t), i = 1, 2, \; r \in \{l \in \mathbb{R} : l\theta_i \in \Omega\}. \tag{26}$$

Because of the identity $a^{\mathbf{E}}(r\theta_i) = a^{1/H_i}(r\theta_i)$ for all $a > 0$ we get

$$\xi_{\theta_i}(ar) \stackrel{d}{=} a^{H_i}\xi_{\theta_i}(r), \tag{27}$$

so $\xi_{\theta_i}(r)$ is self-similar with Hurst index H_i. The anisotropy in space of our random field is determined by the direction of θ_1, θ_2 as well as the ratio between H_1 and H_2 as shown in Figs. 2 and 3. The special case of isotropy is only given when $\theta_1 \cdot \theta_2 = 0, H_1 = H_2$, see Figs. 4 and 5. In both combinations of eigenvectors the spatial range dependence raises with values of H_1 and H_2.

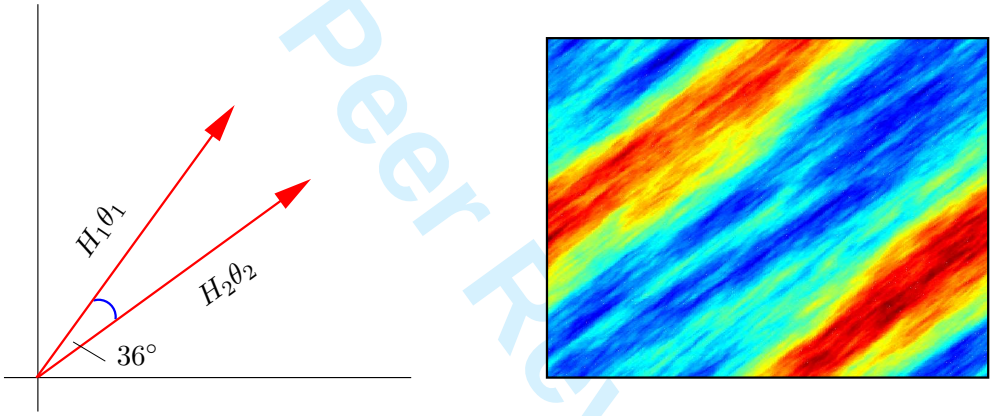

Figure 2.: Anisotropic behavior of ξ given by $\theta_1 = e^{i\cdot 0.3\pi}$, $\theta_2 = e^{i\cdot 0.2\pi}$, $H_1 = H_2 = 0.5$. The colors describe the intensity/magnitude of ξ (at a fixed time).

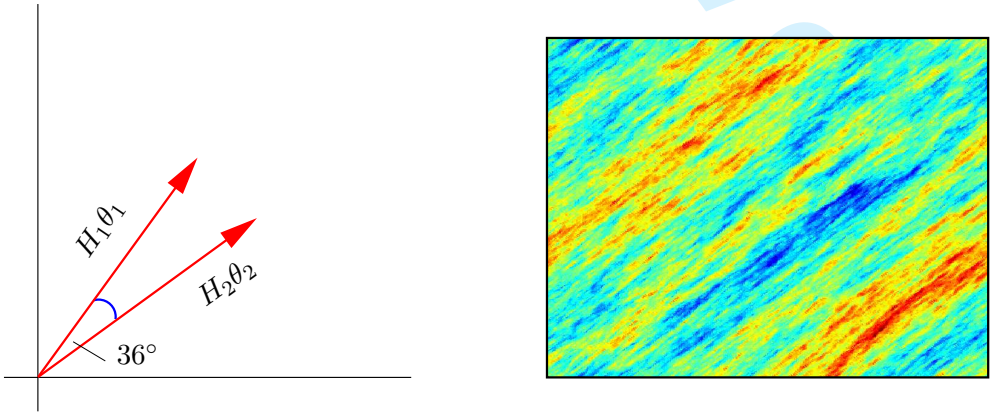

Figure 3.: Anisotropic behavior of ξ given by $\theta_1 = e^{i\cdot 0.3\pi}$, $\theta_2 = e^{i\cdot 0.2\pi}$, $H_1 = H_2 = 0.35$. The colors describe the intensity/magnitude of ξ (at a fixed time).

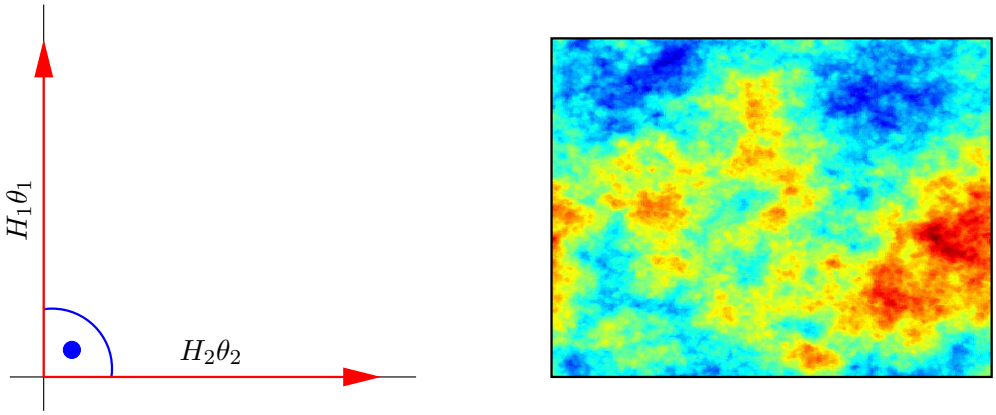

Figure 4.: Isotropic behavior of ξ given by $\theta_1 = e^{i\frac{\pi}{2}}$, $\theta_2 = e^{i\cdot 0}$, $H_1 = H_2 = 0.5$. The colors describe the intensity/magnitude of ξ (at a fixed time).

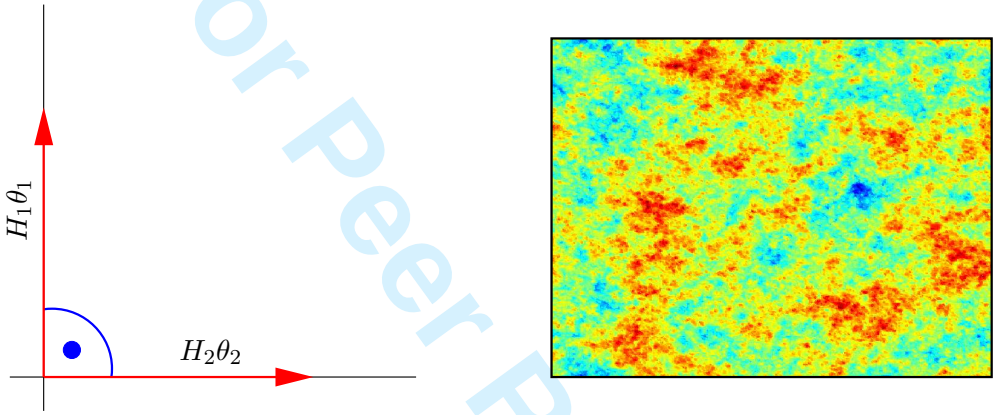

Figure 5.: Isotropic behavior of ξ given by $\theta_1 = e^{i\frac{\pi}{2}}$, $\theta_2 = e^{i\cdot 0}$, $H_1 = H_2 = 0.35$. The colors describe the intensity/magnitude of ξ (at a fixed time).

3.2. *Examples*

Let us present two simulations of random fields which will be used in a similar form in section 5. The first example is a realization of an isotropic random field with parameters

$$H_1 = H_2 = 0.6,\ H_3 = 1.0,\ \theta_1 = (1, 0),\ \theta_2 = e^{i\frac{\pi}{2}}. \tag{28}$$

This field, shown in Fig. 6, has no orientation and because of the term $(e^{i(t_{\max}-t)s}-1)$ in (18) the intensity of the field is decreasing until zero at time $t_{\max}$.
Finally, we want to present an anisotropic field with an orientation of 135° and long range dependence in space. We use the following parameter set

$$H_1 = 0.55,\ H_2 = 0.4,\ H_3 = 0.75,\ \theta_1 = e^{i\frac{3\pi}{4}},\ \theta_2 = e^{i\left(\frac{3\pi}{4}+0.1\frac{\pi}{4}\right)} \tag{29}$$

and get the desired field as shown in Fig. 7. In both simulations the activity period of the random field is set by $t_{\max} = 0.002$.

3.3. *Operator-scaling anisotropic random fields in material science*

Operator-scaling anisotropic random fields may look very academic at the first glance as they are extremely sophisticated with regard to their formal structure.

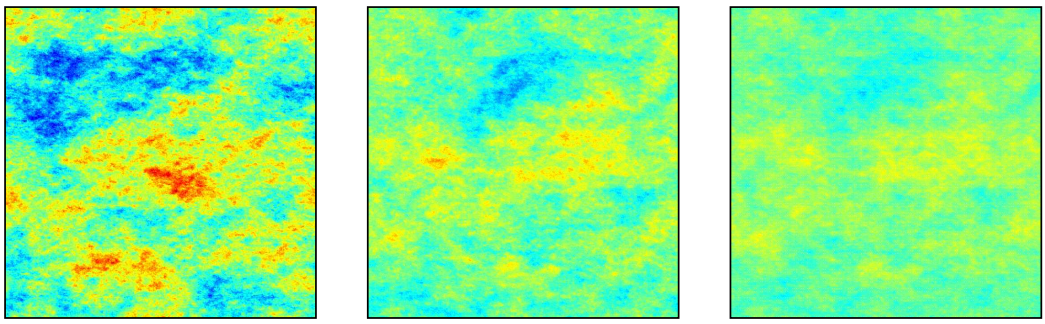

$t = 0$ $t = 0.00145$ $t = 0.0017$

Figure 6.: Simulation of a fully isotropic random field with a smoothly decreasing intensity over a short period of time ($t_{\max} = 0.002$).

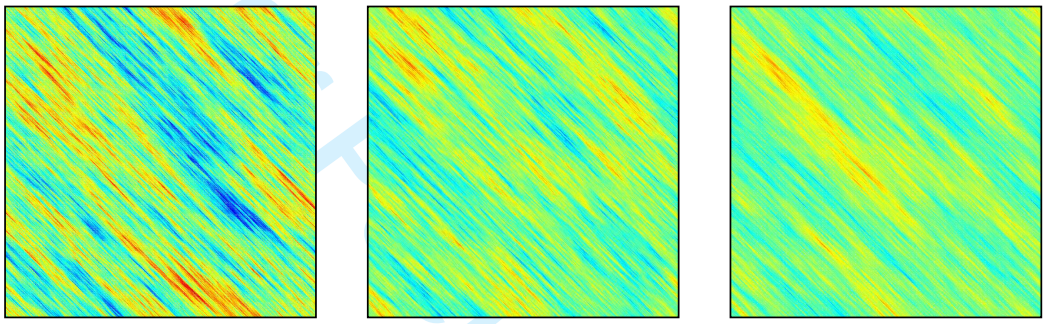

$t = 0$ $t = 0.00145$ $t = 0.0017$

Figure 7.: Simulation of an anisotropic random field with an orientation of 135° and a smoothly decreasing intensity over a short period of time ($t_{\max} = 0.002$).

However, their general scaling properties in time and space correspond to observations of physical phenomena in technically relevant production processes (e.g. within the area of material science). In many technical applications of materials it is vital to capture the microstructural evolution during the production process, which is determined by random nucleation and subsequent growth mechanisms such as spinodal decomposition and Ostwald ripening. As the evolving microstructures usually exhibit non-equilibrium features, their current arrangement is not exclusively determined by current process parameters and material properties, but also by preceding processes in microstructural formation. Therefore, random fields which are uncorrelated in time as classical Brownian motion and Gaussian white noise cannot reproduce this temporal correlation of microstructural evolution. A physical process which has a clear random character is *heterogeneous nucleation*. Actually, it is not practicable to capture both nucleation and growth processes at the same time, because nucleation events require an extremely small resolution in time and space increasing dramatically the computational cost to describe mesoscopic growth. For this reason diffuse-interface models as we will employ in this context, describe nucleation events as local fluctuations or inhomogeneities in properties like composition/density or the material response to external forcing. In the scope of our manuscript we will employ operator-scaling anisotropic random fields to address local fluctuations with physically reasonable properties in terms of long-range spatial and temporal dependence. A comprehensive overview on techniques to incorporate nucleation into phase-field simulation may be found in [44].

4. Formulation of the extended diffusion model

In this part of our contribution we present the considered diffusion model, which is now extended by an external random driving force ξ, and derive the variational formulation of the problem. Similar to Eq. (3) one obtains

$$\begin{aligned}\frac{\partial c}{\partial t} &= -\nabla\cdot\mathbf{j}+\xi\left(\mathbf{x},t\right)=\nabla\cdot\left(\mathbf{M}\nabla\mu\right)+\xi\left(\mathbf{x},t\right)\\ &=\nabla\cdot\left(\mathbf{M}\nabla\left(\partial_c\Psi^{\mathrm{con}}-\lambda\Delta c\right)\right)+\xi\left(\mathbf{x},t\right)\quad\text{with}\ \ \left(\mathbf{x},t\right)\in\Omega\times\left[0,\mathcal{T}\right],\end{aligned}\tag{30}$$

where $\xi\left(\mathbf{x},t\right)$ is given in (22). Remark that in our formulation ξ is no longer related to a noisy mass current. The chemical potential μ is defined as $\mu=\delta_c\Psi$. In contrast to Cook's model we use here a mobility, which depends on the mixture's composition according to thermodynamical considerations [15, 24, 25, 38]. Unlike the experimental data on diffusion coefficients, mobilities are usually not directly available in literature. Therefore, we follow an approach outlined by Küpper and Masbaum [40], which was also employed by Dreyer and Müller in their computational studies of Sn-Pb alloys [25], to address mobility by values from diffusion coefficients. It is a rather heuristic approach to Fickian type diffusion phenomena. We assume that the chemical potential μ is proportional to the first derivative of the configurational free energy density Ψ^{con} with respect to the composition c. This assumption is physically motivated by the fact that the early stages of phase separation are driven by a minimization of configurational energy. Then there follows a proportionality to the mass current $\mathbf{j}$ according to

$$\mathbf{j}=-\mathbf{M}\nabla\mu\approx-\mathbf{M}\nabla\left(\partial_c\Psi^{\mathrm{con}}\right)=-\mathbf{M}\partial_c^2\Psi^{\mathrm{con}}\nabla c.\tag{31}$$

Since we assume Fickian type diffusion it holds

$$-\mathbf{M}\partial_c^2\Psi^{\mathrm{con}}\nabla c=-\mathbf{D}\nabla c.\tag{32}$$

A juxtaposition of coefficients gives the required relation between the mobility and diffusion tensor

$$\mathbf{M}=\left(\partial_c^2\Psi^{\mathrm{con}}\right)^{-1}\mathbf{D}.\tag{33}$$

This result considers also anisotropic diffusion due to the tensorial character of $\mathbf{M}$ and $\mathbf{D}$. In the scope of this manuscript we choose the following isotropic mobility representation

$$\mathbf{M}=\mathbf{M}\left(c\right)=\frac{D}{\partial_c^2\Psi^{\mathrm{con}}}\mathbf{I},\tag{34}$$

where D is the averaged tracer diffusivity of the mixture in units of $\left[\mathrm{m}^2/\mathrm{s}\right]$. The second derivative of the configurational free energy density $\partial_c^2\Psi^{\mathrm{con}}$ has a unit of $\left[\mathrm{J}/\mathrm{m}^3\right]$. Consequently the mobility expression has always a unit of $\left[\mathrm{m}^5/\left(\mathrm{J\,s}\right)\right]$. Such a definition of the mobility focuses/drives the diffusion process to the interfacial areas, where the second derivative of the configurational free energy density has its minimum. To complete the description of the extended diffusion equation (30) we need to specify the representation of the configurational energy density Ψ^{con}. For a thermodynamically consistent formulation of Ψ^{con} we follow the common Flory-Huggins theory of mixing [29, 36]. For a system where only binary interactions take

place Ψ^{con} can be formulated as

$$\Psi^{\mathrm{con}}(c) = g_1 c + g_2(1-c) + g_3 RT\left[c\ln c + (1-c)\ln(1-c)\right] + \chi c(1-c). \quad (35)$$

The first two terms of the configurational energy (35) express the free energy of the individual components. The third term $g_3 RT\left[c\ln c + (1-c)\ln(1-c)\right]$ represents the entropy of mixing with system's absolute temperature T and gas constant $R = 8.314472\,\mathrm{J/(mol\,K)}$. Since we regard the mixture to be non-ideal, the last term $\chi c(1-c)$ accounts for the excess energy. The material specific parameters g_1, g_2, g_3 and χ are calculated from a curve fitting algorithm to match experimentally measured energy values.
The initial concentration profile is assumed to be known as $c(\mathbf{x},t) = c_0(\mathbf{x})$. In our model the initial concentration will be randomly generated such that

$$c_0(\mathbf{x}) = \bar{c}^{\mathrm{eut}} + r \text{ with } |r| \leq 0.01, \quad (36)$$

where $\bar{c}^{\mathrm{eut}}$ is the constant eutectic concentration and r is a random variable with uniform distribution. To guarantee the conservation of mass in the deterministic part of Eq. (30) and the natural boundary conditions from the variation of Ψ, we prescribe homogeneous Neumann boundary conditions

$$\mathbf{j}\cdot\mathbf{n} = \mathbf{M}\nabla\mu\cdot\mathbf{n} = \mathbf{M}\nabla\left(\partial_c\Psi^{\mathrm{con}} - \lambda\Delta c\right)\cdot\mathbf{n} = 0 \quad \text{in } \partial\Omega\times[0,\mathcal{T}] \quad (37)$$

$$\nabla c\cdot\mathbf{n} = 0 \quad \text{in } \partial\Omega\times[0,\mathcal{T}]. \quad (38)$$

For the numerical approximation of the extended diffusion model by means of a finite element scheme Eq. (30) has to be transferred into a variational formalism. For this purpose Eq. (30) is multiplied by a variation $\delta c \in H^2(\Omega)$. $H^2(\Omega)$ denotes here the Sobolev space of square integrable functions with square integrable derivatives of first and second order. Applying Green's first identity (integration by parts) and making use of the homogeneous boundary conditions (37,38) provides the weak form of the problem: Find $c \in H^2(\Omega)$ such that

$$\begin{aligned}\int_\Omega \frac{\partial c}{\partial t}\delta c\,\mathrm{d}\Omega = -\Big(&\int_\Omega \mathbf{M}\partial_c^2\Psi^{\mathrm{con}}\nabla c\nabla\delta c\,\mathrm{d}\Omega + \lambda\int_\Omega \partial_c\mathbf{M}\Delta c\nabla c\nabla\varphi\,\mathrm{d}\Omega \\ &+\lambda\int_\Omega \mathbf{M}\Delta c\Delta\delta c\,\mathrm{d}\Omega\Big) + \int_\Omega \xi\delta c\,\mathrm{d}\Omega \qquad \forall\,\delta c\in H^2(\Omega).\end{aligned} \quad (39)$$

Since this primal variational formulation mandates the discrete solution space $\mathcal{V}^h$ to be at least H^2-conforming with $\mathcal{V}^h \subset H^2(\Omega)$, the finite element basis functions need to be piecewise smooth and globally at least C^1-continuous.

To meet the higher requirement in continuity non-standard basis functions have to be employed. For this reason we follow here the spirit of isogeometric finite element analysis [1, 21, 32] and employ non-uniform rational B-spline functions (NURBS). Similar to isoparameteric finite elements, where the function spaces of the geometry approximation and the solution space for the physical problem coincide, the isogeometric finite element formulation makes use of shape functions which are primarily used in computer aided design. In this way the shape functions precisely represent the geometry of the problem even in a coarse model. This sophisticated geometry approximation is not needed in our model, in opposite, for rectangular domains NURBS reduce to simple B-splines in the usual tensor-product form. However, the continuity and smoothness properties of spline functions result

in superior convergence properties of our analysis.
Another attribute that makes this analysis attractive for the application to phase-field methods [6, 47] is the so-called k-refinement process. During k-refinement the order of the approximation functions is increased, comparable to the p-method in the standard finite element methodology. But in contrast to the p-method the continuity/smoothness is increased as well. Therefore spline based finite element techniques can be exploited for an accurate and robust approximation of problems involving higher-order differential operators.
Facing these benefits, we use a NURBS-based Galerkin-type scheme for the spatial approximation of Eq. (39). For the temporal discretization we employ an implicit Crank-Nicholson scheme, which is known to perform a second-order accuracy. For a detailed mathematical description of the approximation procedure and its advantages over other numerical schemes we refer to earlier work, cf. [1–4].

5. Numerical experiments

In this section we investigate the performance of our numerical approximation scheme for the diffusion within a binary mixture driven by a perturbing random field. We restrict our studies to a rather simple rectangular domain Ω in order to focus our attention on the physical and numerical aspects of the problem. To demonstrate the applicability of our stochastic diffusion model, we present numerical results which qualitatively reproduce the scenario observed during thermal aging experiments of an Sn-Pb solder in eutectic composition, cf. Fig. 8. In the micrographs the light (gray) areas denote the tin-rich matrix phase and the dark (black) areas characterize the lead-rich particle phase.

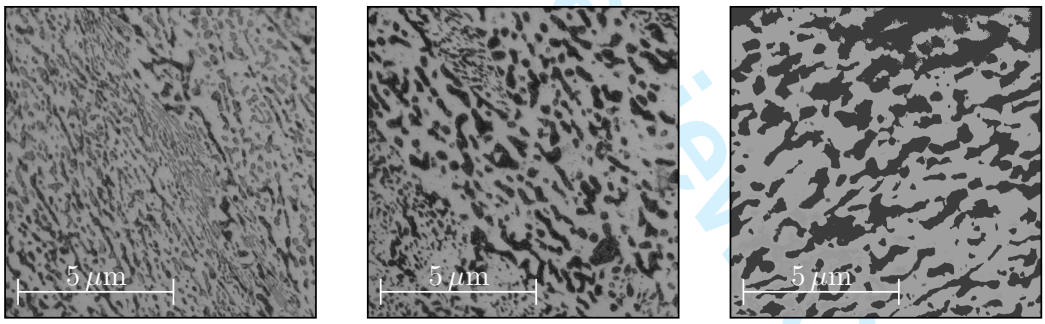

$t = 2\,\mathrm{h}$ $t = 16\,\mathrm{h}$ $t = 60\,\mathrm{h}$

Figure 8.: Micrographs from aging experiments of eutectic Sn-Pb at an operating temperature of 150 °C. Here t denotes the time after solidification.

The solder under consideration contains on average 63% Sn and 37% Pb. The operating temperature during experiments was kept constant at 150 °C ($T = 423.16\,\mathrm{K}$). The specific material properties enter the diffusion equation by the following set of material parameters

$g_1\ \left[\frac{\mathrm{GJ}}{\mathrm{m}^3}\right]$	$g_2\ \left[\frac{\mathrm{GJ}}{\mathrm{m}^3}\right]$	$g_3\ \left[\frac{\mathrm{mol}}{\mathrm{m}^3}\right]$	$\chi\ \left[\frac{\mathrm{GJ}}{\mathrm{m}^3}\right]$	λ [N]	c_α	c_β	$\bar{c}^{\mathrm{eut}}$
-1.5248	-1.3429	$7.2711 \cdot 10^4$	0.8565	$2.57 \cdot 10^{-7}$	0.0455	0.9545	0.37

Table 1.: Material specific parameters for an eutectic Sn-Pb alloy.

The parameters g_1, g_2, g_3 and χ are chosen in such a way that the resultant free energy density Ψ^{con} achieves an optimal fit to the experimentally measured energy data. The shape of the configurational energy density Ψ^{con} and the common tangent characterizing the equilibrium phases is illustrated in Fig. 9. During our simulations the concentration field is identified with the mass fraction of lead (Pb), i.e. a material volume with $c = 0$ consists of pure (100%) tin (Sn) and a material volume with $c = 1$ of 100% lead. For this system, islands of the Pb-rich β-phase c_β evolve within a Sn-rich α-phase (c_α) matrix.

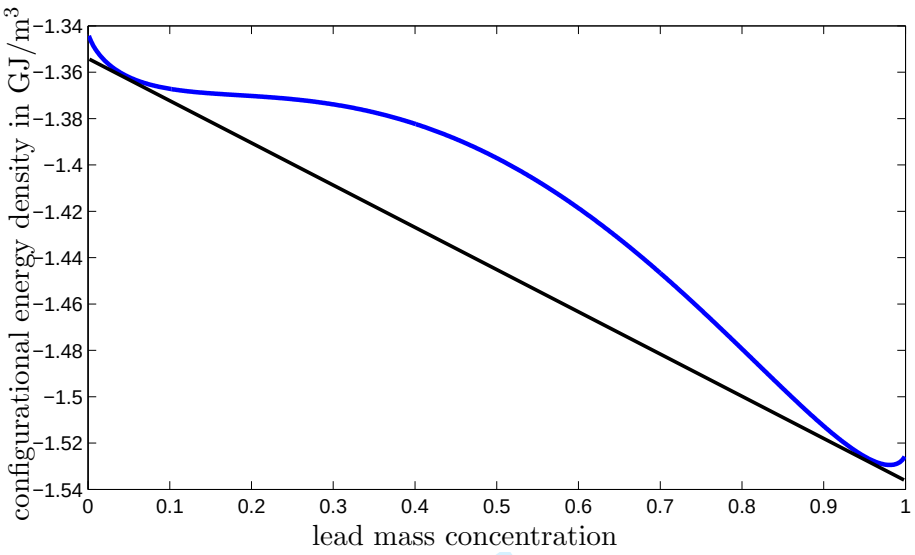

Figure 9.: Shape of configurational energy density Ψ^{con} (blue curve) and the corresponding common tangent (black line).

The kinetic properties of the system are determined by the temperature dependent diffusion coefficient D, which is given by an Arrhenius equation

$$D = D_0 e^{\frac{-\mathcal{E}_a}{RT}}, \tag{40}$$

where D_0 is an extrapolated (academic) diffusion coefficient at infinite temperature, $\mathcal{E}_a$ denotes the activation energy of the diffusion process, R is the universal gas constant and T is the system's temperature. In order to obtain the required data for the Arrhenius relation, we refer to studies of Gupta et al. [33] and Decker et al. [23]. In their contributions the activation energy is measured as $\mathcal{E}_a = 100\,\text{kJ/mol}$ and the pre-exponential diffusivity D_0 varies from $2.5-6.7\cdot10^{-5}\,\text{m}^2/\text{s}$. In our model we take $D_0 = 6.5 \cdot 10^{-5}\,\text{m}^2/\text{s}$. Please keep in mind that the presented parameters are measured on a slightly higher temperature level than it is assumed in our investigation. According to the model of a degenerate mobility (34) in combination with the representation for Ψ^{con} used in our manuscript (35) we obtain

$$\mathbf{M}(c) = \frac{D}{\partial_c^2 \Psi^{\text{con}}}\mathbf{I} = \frac{c(1-c)}{g_3 RT - 2\chi c(1-c)}\mathbf{I}. \tag{41}$$

To avoid unphysical singularities of mobility in the spinodal points where $\partial_c^2 \Psi^{\text{con}}$ vanishes, the mobility expression is regularized in such a way that the term

$2\chi c\,(1-c)$ is omitted. This regularization yields

$$\mathbf{M}\,(c) = \frac{D}{\partial_c^2 \Psi^{\mathrm{con}}}\mathbf{I} = \frac{Dc\,(1-c)}{g_3 RT}\mathbf{I} = Mc\,(1-c)\,\mathbf{I}. \tag{42}$$

Consequently, the isotropic mobility coefficient M is e.g., given by $M = 1.03 \cdot 10^{-25}\,\mathrm{m}^5/\,(\mathrm{J\,s})$. This value corresponds to the mobility coefficient employed by Ubachs et al. [47] during the numerical investigation of an eutectic tin-lead solder in a similar configuration as it is assumed in this manuscript. Please note that the constant part of $\partial_c^2 \Psi^{\mathrm{con}}$ was omitted in (42) for convenience.

At first, we present simulation results for the deterministic diffusion model, which will illustrate the limitations of this model. Hereafter simulation results obtained for the stochastic diffusion model will demonstrate the decisive advantages of this model. All numerical studies employ the characteristic reference length $\mathfrak{L} = 5\,\mu\mathrm{m}$ for the spatial coordinates and $\mathcal{T} = 67.4\,\mathrm{h}$ for the temporal scale. By means of these length-scales we can introduce dimensionless coordinates

$$\mathbf{x}^* = \frac{\mathbf{x}}{\mathfrak{L}}, \quad t^* = \frac{t}{\mathcal{T}} \tag{43}$$

and reformulate the considered diffusion equation into a dimensionless representation.

5.1. *Simulations of the deterministic diffusion model*

For the simulation of the microstructural evolution within the deterministic regime we employ the presented material parameters and assume $\xi = 0$. In this situation one observes the typical scenario of isotropic spinodal decomposition followed by Ostwald ripening. Starting from an approximately homogeneous mixture, the system is quenched into a thermodynamically unstable state. To leave this unfavorable configuration the mixture commences to separate into phases that minimize the configurational energy with respect to a common tangent (Maxwell tangent rule). After the separation of phases into the equilibrium Pb-rich β-phase (reddish particles) and Sn-rich α-phase (blue matrix) is finished, the evolved particles begin to coalesce driven by a tendency to minimize the interfacial/surface energy. This process where the bigger particles grow at the cost of smaller particles is referred to as Ostwald ripening.
Simulation results for the early stages of spinodal decomposition are illustrated in Fig. 10. We observe a decomposition with round β-phase particles which will coalesce and grow. The process of phase coarsening and Ostwald ripening is presented in Fig. 11. The rectangular shape of the phase islands in the late stages results from a minimization of surface energy. The squared form of the bigger particles constitutes an intermediate configuration before a circular shape is adopted in the very late stationary equilibrium. This effect may look unphysical but is inherent in the *idealized* Cahn-Hilliard-theory. Rectangular particles which are present in states near stationary equilibrium usually stem from anisotropy and mechanical effects, cf. [30].

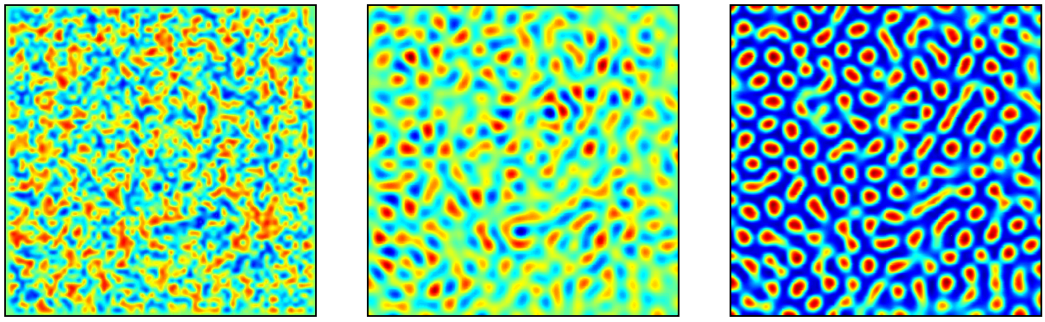

$t^* = 0$ $t^* = 0.005$ $t^* = 0.0125$

Figure 10.: Simulation results for spinodal decomposition within the deterministic diffusion model.

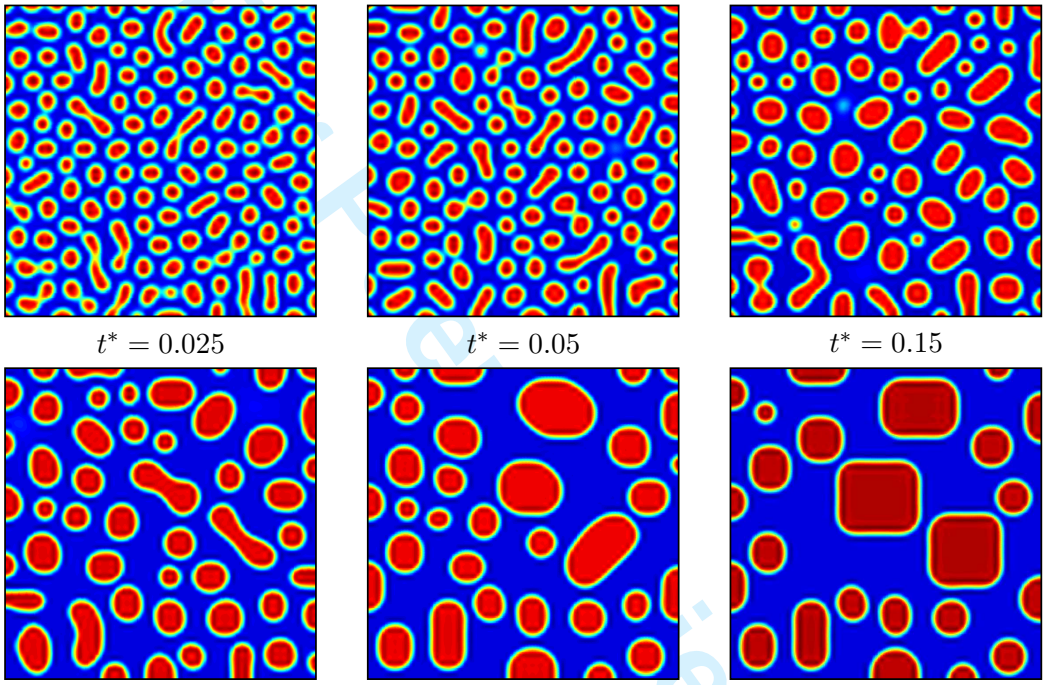

$t^* = 0.025$ $t^* = 0.05$ $t^* = 0.15$

$t^* = 0.35$ $t^* = 3.0$ $t^* = 12.55$

Figure 11.: Simulation results for the early and late stages of Ostwald ripening within the deterministic diffusion scenario.

5.2. *Simulations of the stochastic diffusion model*

In order to include anisotropic random fluctuations into the diffusion model the noise contribution ξ as given by Eq. (22) is no longer equal to zero. The random noise is written in units of s^{-1}. During all our numerical simulations the imposed random fields are only present during spinodal decomposition and the very early stages of phase coarsening, where the mixture is most susceptible to external fluctuations.

In the first example we intend to depict the evolution of randomly contorted particles during spinodal decomposition. This objective can be accomplished by an almost isotropic random field with long-range dependence in temporal and spatial coordinates. The corresponding parameter set for this random field reads

$$H_1 = H_2 = 0.35,\ H_3 = 1.0,\ \theta_1 = (1, 0),\ \theta_2 = e^{i\pi/2}. \tag{44}$$

Again the simulation initiates from a homogeneous state which is cooled into the unstable spinodal regime. The influence of the imposed random field during spinodal decomposition is apparent. From the very first time step the concentration field follows the random driving with a slight temporal shift, cf. Fig. 12. Due to the noise contribution a morphology evolves that conforms with the irregular experimental microstructure in Fig. 8 in contrast to the regular spherical and elliptic phase islands in the deterministic simulation. The simulated microstructure shows after the separation of phases a typical coarsening behavior, see Fig. 13.

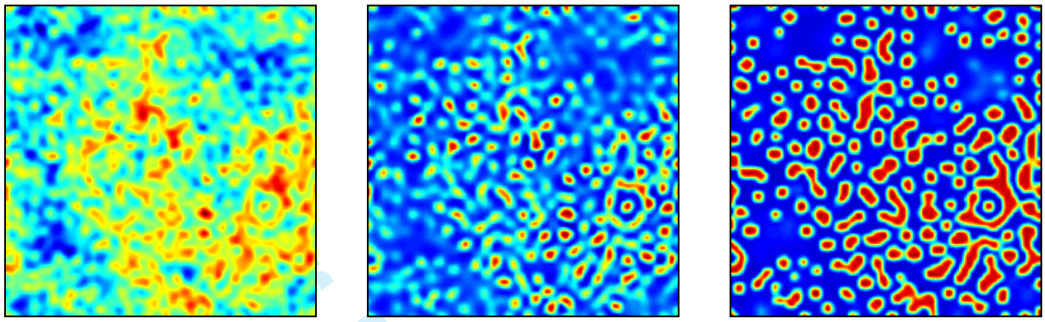

$t^* = 0.0015$ $t^* = 0.0035$ $t^* = 0.0055$

Figure 12.: Evolution of contorted particles during the early stages of spinodal decomposition within the stochastic diffusion scenario ($t_{\max} = 0.00375$).

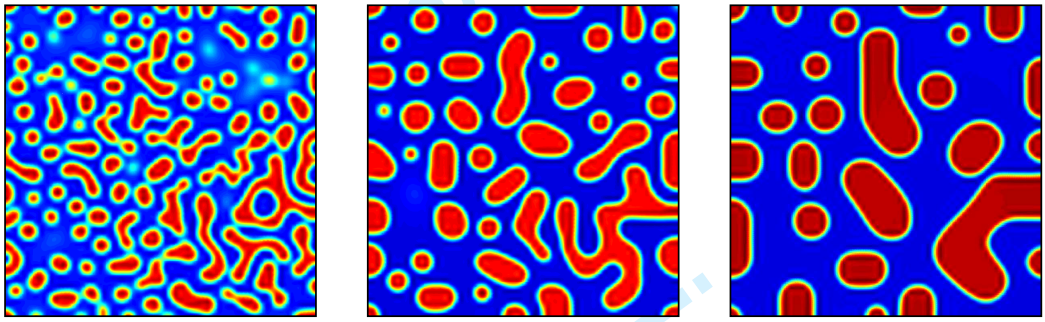

$t^* = 0.0455$ $t^* = 0.1805$ $t^* = 2.0$

Figure 13.: Evolution of contorted particles during the early stages of Ostwald ripening within the stochastic diffusion regime ($t_{\max} = 0.00375$).

To provide a sound and meaningful comparison between the stochastic and deterministic diffusion model, we investigate the coarsening rate by means of the temporal evolution of the average particle radius and the decrease of interfacial area. It is *very* complicated to find a reasonable measure to qualify microstructural evolution and coarsening. As reference solution we therefore have recourse to the Lifshitz-Slyozov-Wagner (LSW) theory [43, 49] which provides for the average radius $\bar{r}$ of the evolving particles the well-known proportionality $\bar{r} \propto t^{\frac{1}{3}}$. Here, one must be aware that the LSW theory is only valid in supersaturated (dilute) solutions within a low volume fraction regime. The LSW theory describes in general an isotropic coarsening without any driving forces such as mechanical and thermal fields. We assume that coarsening processes in our systems can be partly captured by this theory. Another measure to quantify the rate of coarsening is the decrease of interfacial area which is proportional to the surface/gradient energy because the surface/gradient energy is entirely stored within the interfaces. It is a rather intuitive and heuristic approach to characterize coarsening rates in multiphase systems but this idea serves as basis for the derivation of upper and lower bounds for the

decrease in surface energy during Ostwald ripening, cf. [17, 45].

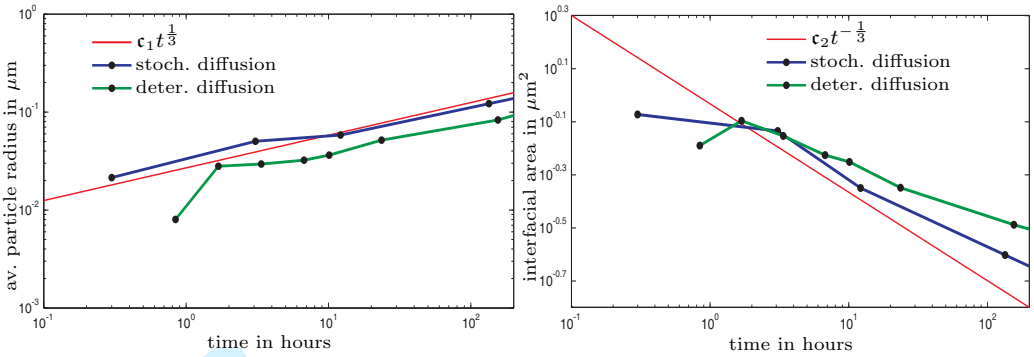

Figure 14.: Comparison of the temporal evolution of average particle radius and interfacial area in the deterministic and stochastic diffusion model.

The comparison of coarsening rates in the deterministic Cahn-Hilliard equation and the isotropic stochastic diffusion model shows that both models reproduce quite well the physics of Ostwald ripening in the very late stages of microstructural evolution ($t > 50\,\mathrm{h}$). Nevertheless, the discrepancies of the deterministic model become obvious during spinodal decomposition and in the early stages of Ostwald ripening ($t < 5\,\mathrm{h}$), where the average particle radius increases much faster than the growth law $\mathfrak{c}_1 t^{1/3}$. Due to the incorporation of random effects from solidification for the very early stages of phase separation the stochastic diffusion system complies from the beginning of our simulation with the growth law. The randomly induced formation of irregular clusters of particles leads to an improved behavior in the decrease of interfacial area, which is for $t > 3\,\mathrm{h}$ slightly faster than the decrease of interfacial area within the deterministic framework.

In the second example we present a fully anisotropic random field with an average orientation of $-45°$. In this configuration it is possible to reproduce the oriented lamellae structure as it is locally observed during the aging experiments of eutectic Sn-Pb, cf. Fig. 15. The lamellar microstructure evolves predominantly during the early stages of spinodal decomposition. In the later coarsening stages these structures coalesce and a clear orientation cannot be recognized anymore.

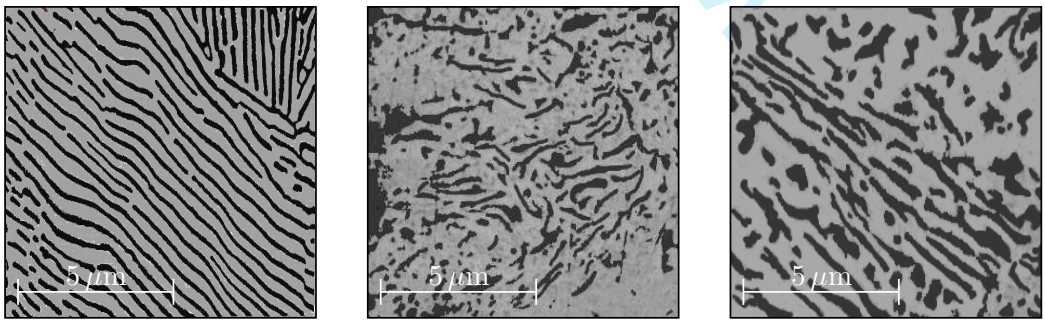

$t = 2\,\mathrm{h}$ $t = 6\,\mathrm{h}$ $t = 12\,\mathrm{h}$

Figure 15.: Micrographs of lamellar structures observed during aging experiments of an eutectic Sn-Pb solder.

The required parameters for the underlying random field are

$$H_1 = 0.35,\ H_2 = 0.4,\ H_3 = 0.75,\ \theta_1 = e^{-i\frac{1}{4}\pi},\ \theta_2 = e^{-i\frac{1.02}{4}\pi}. \qquad (45)$$

The recorded simulation results for the microstructural evolution driven by a lamellar random field are convincing at the first glance. Right from the start of the unmixing process the concentration field is forced into lamellar structures with an average orientation of $-45°$ as anticipated, see Fig. 16. After the influence of the random field vanishes at $t^* = 0.00375$ the process of phase separation is finished at $t^* = 0.0075$ and a minimization of the interfacial energy is initiated as usual. This can be seen in a growing thickness of each lamella. We remark that the application of an external random field accelerates the initial separation dynamics compared to the deterministic model, cf. Fig. 10.

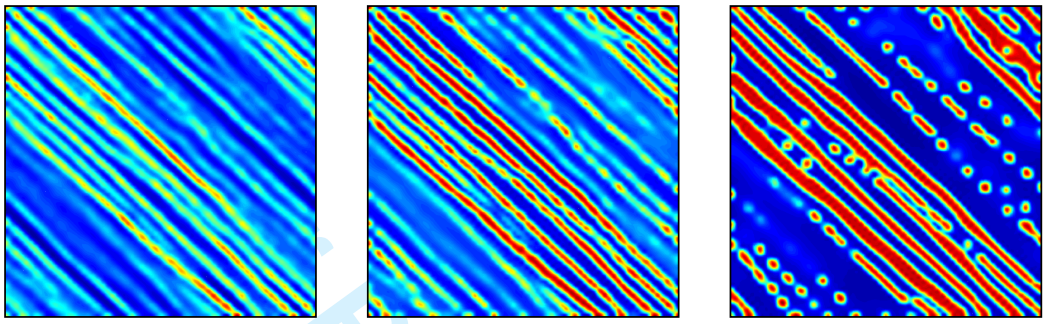

$t^* = 0.0025$ $t^* = 0.00375$ $t^* = 0.0075$

Figure 16.: Evolution of lamellar microstructure during the early stages of spinodal decomposition within the stochastic diffusion model ($t_{\max} = 0.00375$).

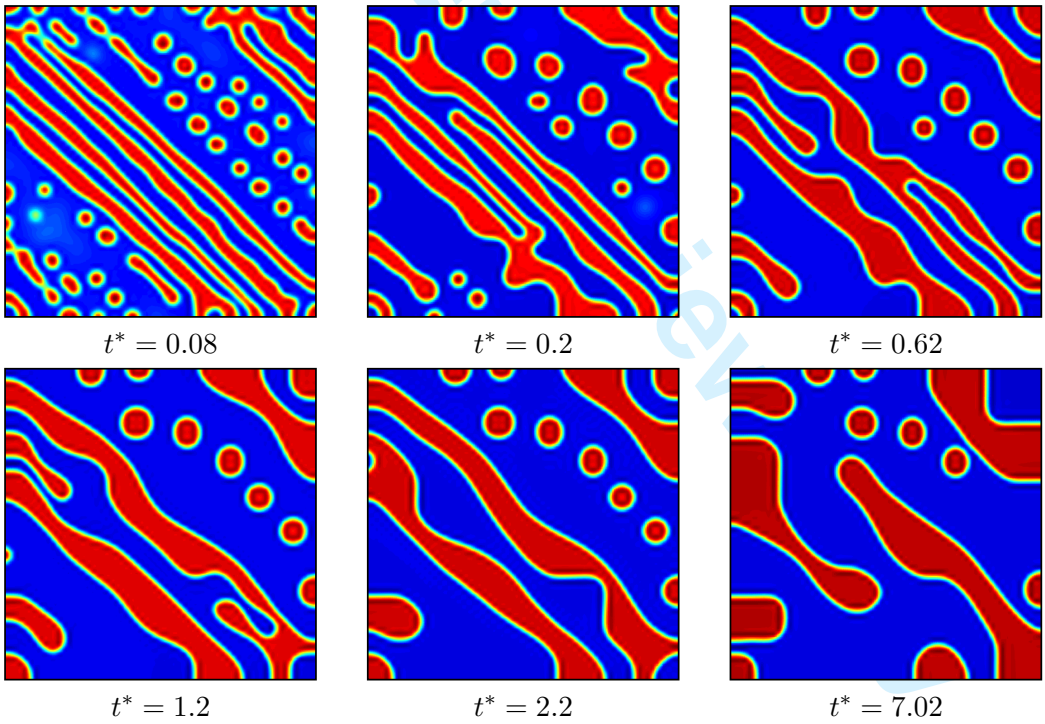

$t^* = 0.08$ $t^* = 0.2$ $t^* = 0.62$

$t^* = 1.2$ $t^* = 2.2$ $t^* = 7.02$

Figure 17.: Different stages of phase coarsening in a lamellar microstructure induced by an anisotropic random field.

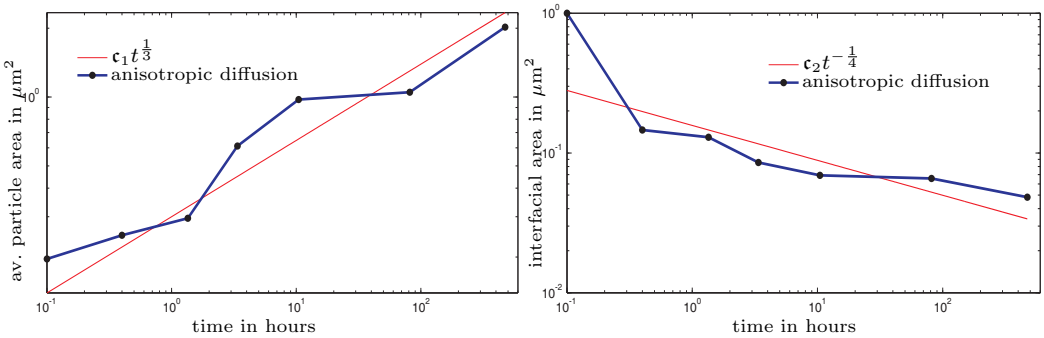

Figure 18.: Temporal evolution of average particle/lamellae area and interfacial area versus several growth laws.

Since the classical LSW theory with the $t^{1/3}$-power law considers coarsening of isolated, widely spaced particles of one phase embedded within a large matrix phase by the so-called condensation-evaporation mechanism, it directly cannot be applied to the coarsening of highly interconnected, interpenetrating lamellar morphologies. For the quantification of coarsening of lamellar structures it is not meaningful to define an average radius as characteristic length scales. Finite difference and spectral approximation techniques usually employ the autocorrelation of the concentration field in Fourier space which defines a reasonable structure measure. We follow here a different strategy and employ the average lamella/particle size which we regard to be proportional to the product of a dominating length scale and a considerably smaller reference length. As second measure for coarsening we employ again the decrease in interfacial area.

After spinodal decomposition is completed, the early and intermediate stages of phase coarsening ($1\,\mathrm{h} < t < 40\,\mathrm{h}$) are dominated by a faster growth processes than the classical condensation-evaporation mechanism. This effect was studied by Huse in [37], where he formulated a generalized version of the LSW 1/3-growth law for early simulation times of tortuous microstructures. In these lamellar microstructures the coarsening process is enhanced by an additional conductivity of matter via the interfaces. For the later stages of ripening process ($40\,\mathrm{h} \ll t$) the structure asymptotically approaches the 1/3-growth law. Due to the initially anisotropic random forcing the interfacial area decreases with a slightly slower growth law of $\mathfrak{c}_2 t^{-1/4}$.

At this point it should be stated that lamellar and irregularly clustered structures are inherent in the physics of solidification processes. Especially alloys in eutectic composition show a variety of microstructural morphologies. For binary systems one usually distinguishes between four different stereotypes of eutectic morphologies, see Fig. 19.

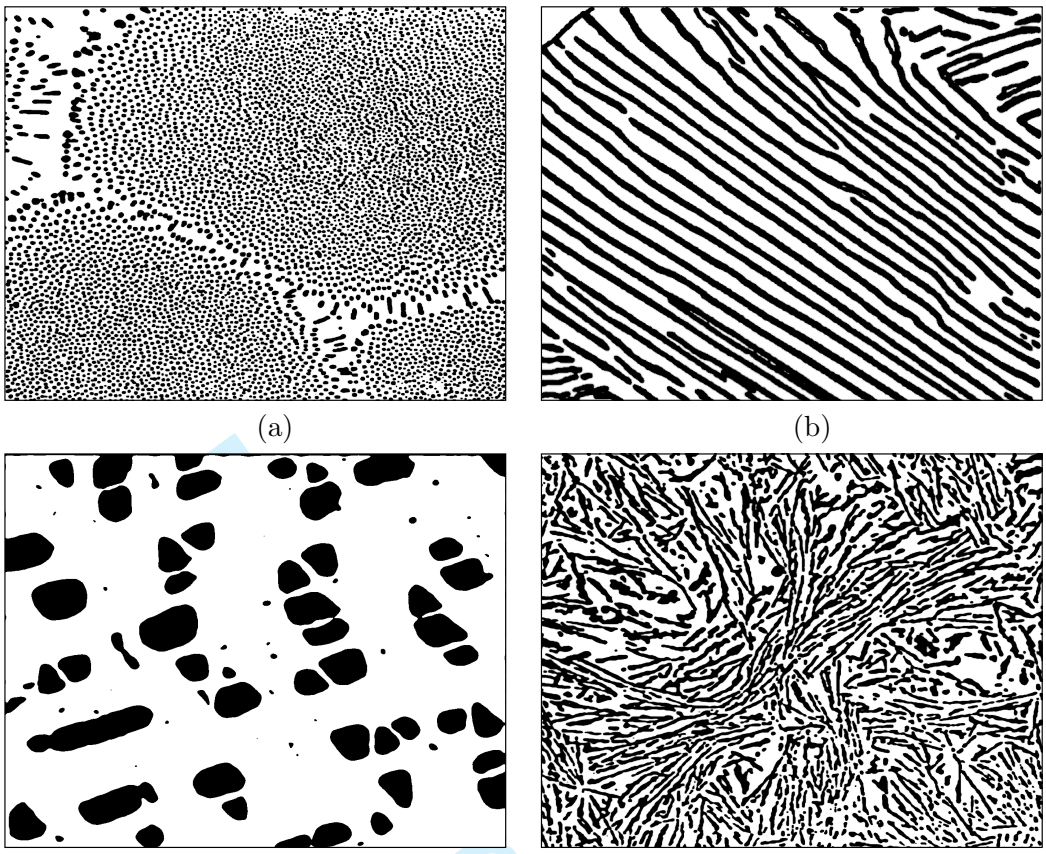

Figure 19.: Schematic illustration of typical eutectic structures: (a) regular, globular or fibrous arrangement, (b) regular lamellar arrangement, (c) irregular faceted fibrous arrangement and (d) irregular lamellar arrangement. Regular microstructural arrangements are preferred when both phases have a low entropy of fusion and isotropic surface energies; in case of a high entropy of fusion the eutectics tend to form irregular structures. A small volume fraction of one phase favors the formation of fibers and globular particles, whereas higher volume fractions of both phases provoke a formation of lamellar structures.

The lamellar microstructure considered in our computational studies results from the (coupled) eutectic growth during solidification. Eutectics are known to arrange in lamellar microstructures – resulting from an interplay of different mechanisms of diffusion and capillary effects during solidification. Further sources of irregular microstructural formation can be found in slight deviations from the ideal eutectic composition. In such cases precipitates of primary α or β-phase evolve in the melt, when the system is cooled until it reaches the liquidus line. Further cooling increases the content of tin in the precipitated α -phase (for $c < c_{\mathrm{eut}}$) or lead is enriched in the precipitated β-phase (for $c > c_{\mathrm{eut}}$). If eutectic temperature is reached, the irregularly precipitated solid phases serve as nuclei for eutectic solidification of the remaining melt. A purely lamellar microstructure can only be achieved if the eutectic composition is kept in the entire system. An illustration of different solidification scenarios for the Sn-Pb system is given in Fig. 20.

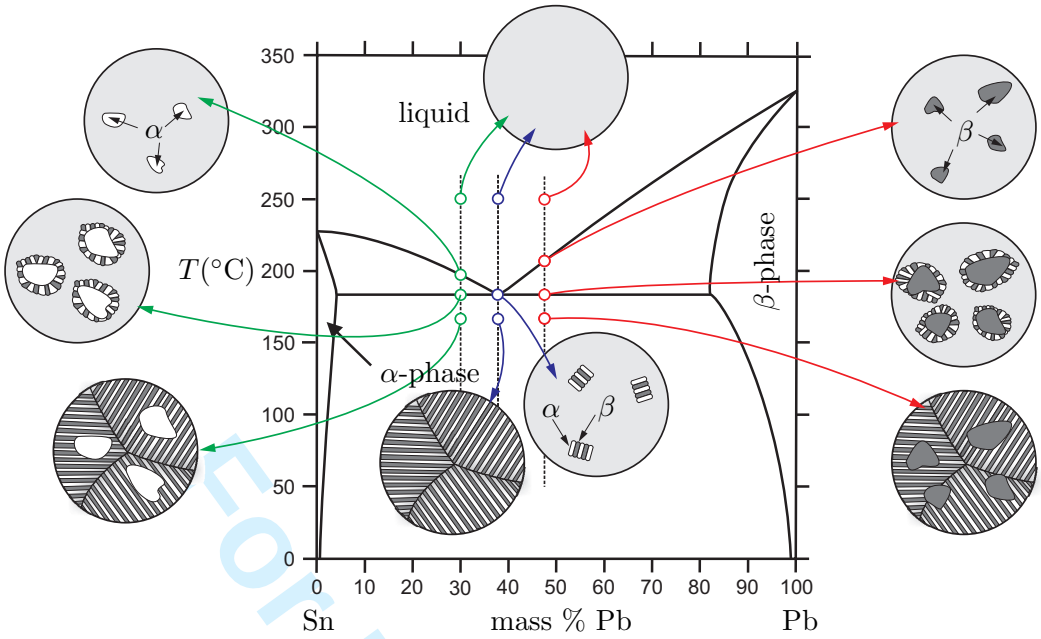

Figure 20.: Phase diagram of a binary Sn-Pb solder alloy. The insets illustrate different solidification scenarios around the eutectic concentration. Here, light gray marks the melt, white the tin-rich α-phase and dark gray the lead-rich β-phase.

Since we have seen that solidification initiates from irregular nucleation and growth, it is an extremely inhomogeneous process involving the occurrence of locally differing crystalline orientation. Therefore the resulting microstructure will be inhomogeneous as well. During experiments it can be seen that the unmixed microstructure exhibits preferentially oriented lamellae. This phenomenon can mathematically be captured by an anisotropic diffusion coefficient. In such models the mobility becomes a tensor

$$\mathbf{M} = \frac{1}{\partial_c^2 \Psi^{\mathrm{con}}} \left(D^{\mathrm{iso}} \mathbf{I} + D^{\mathrm{ani}} \mathbf{a} \otimes \mathbf{a} \right), \tag{46}$$

where D^{iso} is the isotropic diffusivity and D^{ani} denotes the anisotropic diffusion coefficient. $\mathbf{a} \otimes \mathbf{a}$ represents the anisotropic structural tensor with characteristic direction $\mathbf{a}$. The drawback of this approach is that the experimental determination of D^{ani} and $\mathbf{a}$ is cumbersome.

In our approach the local crystalline orientation can be included straight-forward by an appropriate random field. Consequently, our last example incorporates different crystalline orientations into the microstructural evolution. The corresponding random field is arranged in an alveolate crystalline pattern, where each hexagon is subject to a randomly generated set of parameters for the noise contribution. Fig. 21 illustrates a 4×3 hexagonal lattice used during our numerical simulations.

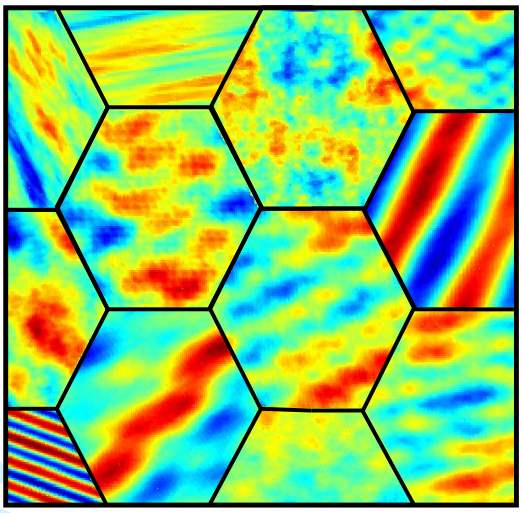

Figure 21.: Illustration of an alveolate crystalline random field with heterogeneous noise contributions within each hexagon at $t^* = 0.0001$. The black lines are for purpose of illustration only.

The induced microstructure clearly mirrors the locally differing random forcing during the very first stages of spinodal decomposition. Since the noise contribution only affects the diffusion process in the initial time steps from $t^* = 0$ up to $t^* = 0.00375$, the emerged phase orientation can be observed at best in this time interval, cf. Fig. 22. After the random field vanished, the phases arbitrarily start to rearrange into clusters of bigger particles and the ordinary coarsening of phases initiates. For this reason further illustrations of the simulated coarsening scenario have been omitted since they do not provide new information.

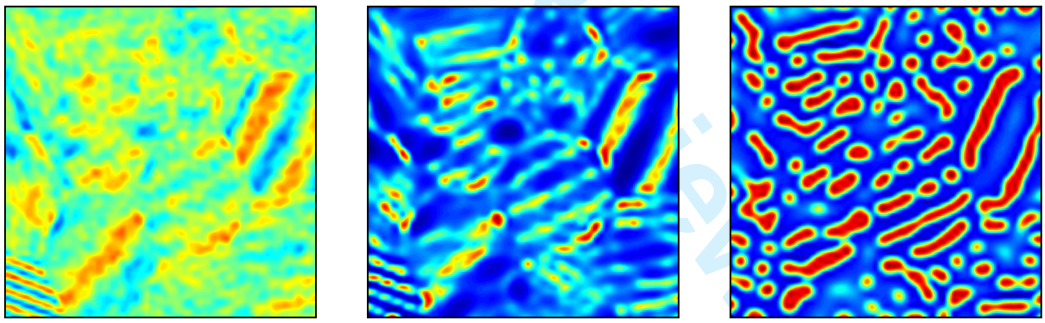

$t^* = 0.00015$ $t^* = 0.001$ $t^* = 0.0075$

Figure 22.: Simulation of anisotropic diffusion subjected to alternating alveolate crystalline orientation.

6. Summary

By now it has become evident that Brownian motion is a too simple description of diffusion processes in complex systems like the rearrangement of particles in the decomposition of mixtures. For this reason, the authors suggest to replace the classical stochastic diffusion model of Cook and Hilliard by a new approach corresponding to a random motion with short-range and long-range interactions and anisotropic scaling. We have shown that this operator-scaling random field extension of the Cahn-Hilliard phase-field model is fully able to map the microstructural evolution

as observed in the experiments. Implemented in the context of isogeometric finite-element analysis our model simulates isotropic as well as locally anisotropic phase arrangements in a realistic way.

We would like to emphasize at this point, that the application of an operator-scaling anisotropic random field does *not* affect the physics of the model. Of course, lamellae like phases and oriented shapes can easily be enforced by an anisotropic material model. For example, the diffusion coefficient and the resulting mobility of the phases may depend on the direction as outlined in Section 5. However, in order to demonstrate the effect of the proposed random fields we restrict our simulations to a purely isotropic phase field evolution. Beyond that, anisotropy of the microstructure may also result from superposed stresses and it can be enforced in a simulation by considering elastic stress or strain fields in the the diffusion model. We have done such simulations but refrain from presenting these in order to point out that all anisotropy we show here is due to a *randomly* fluctuating driving force working within the first few hundredth of the aging period considered.

Appendix A. Fourier transform

In this appendix, we elaborate on the mathematical details concerning the Fourier transform to obtain the amplification factor $\alpha(\mathbf{k})$. First of all we formally define the Fourier transform $\hat{f}$ of a function $f \in L^1(\mathbb{R}^n, \mathbb{C})$ (space of integrable functions) by

$$\hat{f}(\mathbf{k}) := \frac{1}{(2\pi)^{\frac{n}{2}}} \int_{\mathbb{R}^n} e^{-i\mathbf{kx}} f(\mathbf{x}) \, \mathrm{d}\mathbf{x} \qquad \forall \mathbf{k} \in \mathbb{R}^n. \tag{A1}$$

For the derivation of the amplification factor we take the Fourier transform of the deterministic Cahn-Hilliard equation with $\Omega \subset \mathbb{R}^2$ and make use of Green's integral formula:

$$\frac{\partial \hat{c}}{\partial t} = \frac{1}{2\pi} \int_{\mathbb{R}^2} \nabla \cdot \left(M \nabla \left(\partial_c \Psi^{\mathrm{con}} - \lambda \Delta c \right) \right) e^{-i\mathbf{kx}} \, \mathrm{d}\mathbf{x} \tag{A2}$$

$$= -\frac{1}{2\pi} \int_{\mathbb{R}^2} M \nabla \left(\partial_c \Psi^{\mathrm{con}} - \lambda \Delta c \right) (-i\mathbf{k}) \, e^{-i\mathbf{kx}} \, \mathrm{d}\mathbf{x} \tag{A3}$$

$$= \frac{1}{2\pi} \int_{\mathbb{R}^2} M \partial_c^2 \Psi^{\mathrm{con}} \nabla c \, (i\mathbf{k}) \, e^{-i\mathbf{kx}} \, \mathrm{d}\mathbf{x} - \frac{M\lambda}{2\pi} \int_{\mathbb{R}^2} \nabla \Delta c \, (-i\mathbf{k}) \, e^{-i\mathbf{kx}} \, \mathrm{d}\mathbf{x} \tag{A4}$$

$$\overset{*}{=} - \|\mathbf{k}\|^2 M \partial_c^2 \Psi^{\mathrm{con}} \frac{1}{2\pi} \int_{\mathbb{R}^2} c e^{-i\mathbf{kx}} \, \mathrm{d}\mathbf{x} + \|\mathbf{k}\|^2 M\lambda \frac{1}{2\pi} \int_{\mathbb{R}^2} \Delta c e^{-i\mathbf{kx}} \, \mathrm{d}\mathbf{x} \tag{A5}$$

$$= - \|\mathbf{k}\|^2 M \partial_c^2 \Psi^{\mathrm{con}} \frac{1}{2\pi} \int_{\mathbb{R}^2} c e^{-i\mathbf{kx}} \, \mathrm{d}\mathbf{x} - \|\mathbf{k}\|^4 M\lambda \frac{1}{2\pi} \int_{\mathbb{R}^2} c e^{-i\mathbf{kx}} \, \mathrm{d}\mathbf{x} \tag{A6}$$

$$= - \|\mathbf{k}\|^2 M \partial_c^2 \Psi^{\mathrm{con}} \hat{c} - \|\mathbf{k}\|^4 M\lambda \hat{c} = - \|\mathbf{k}\|^2 M \left(\partial_c^2 \Psi^{\mathrm{con}} + \lambda \|\mathbf{k}\|^2 \right) \hat{c} \tag{A7}$$

$$= \alpha(\mathbf{k}) \, \hat{c}(\mathbf{k}, t) \tag{A8}$$

During the transformation $(*)$ the second partial derivative of the configurational energy $\partial_c^2 \Psi^{\mathrm{con}}$ is evaluated in the mean concentration c_0. Therefore we assume it as constant in this very case. Please note that the boundary expressions which are present in Green's first identity vanish because of an application of the Cauchy integral theorem for these line integrals.
Remark that the inverse Fourier transform used for the derivation of Eq. (14) is given in our model by

$$f(\mathbf{x}) := \frac{1}{(2\pi)^{\frac{n}{2}}} \int_{\mathbb{R}^n} e^{i\mathbf{kx}} \hat{f}(\mathbf{k}) \, \mathrm{d}\mathbf{k} \qquad \forall \mathbf{x} \in \mathbb{R}^n. \tag{A9}$$

References

[1] D. Anders and K. Weinberg. Isogeometric analysis of thermal diffusion in binary blends. Comput. Mater. Sci. (2010) article in press.
[2] D. Anders and K. Weinberg. A variational approach to the decomposition of unstable viscous fluids and its consistent numerical approximation. J. Appl. Math. Mech. (2010) article in press.
[3] D. Anders and K. Weinberg. Numerical simulation of diffusion induced phase separation and coarsening in binary alloys. Comput. Mater. Sci. 50(4) (2011) p.1359.
[4] D. Anders and K. Weinberg. Numerical investigation of diffusion induced coarsening processes in binary alloys. IOP Conf. Ser.: Mater. Sci. Eng. 10 012100 (2010).
[5] K. Barros, R. Dominguez and W. Klein. Beyond Cahn-Hilliard-Cook ordering theory: Early time behavior of spatial-symmetry-breaking phase transition kinetics. Phys. Rev. E 79 042104 (2009).
[6] T. Böhme. *Investigations of Microstructural Changes in Lead-Free Solder Alloys by Means of Phase Field Theories*, Dissertationsschrift, Technische Universität Berlin, 2008.

[7] A. Bonami, A. Estrade. Anisotropic analysis of some Gaussian models. J. F. Anal. Appl. 9 (2003) p.215.
[8] D. Benson, M.M. Meerschaert, B. Bäumer and H.P. Scheffler. *Aquifer Operator- Scaling and the effect on solute mixing and dispersion*. Water Resour. Res. 42 W01415 (2006) p.1.
[9] H. Bierme, M.M. Meerschaert, H.P. Scheffler. Operator scaling stable random fields. Stochastic Processes and their Applications. 117 (2007) p.312.
[10] R. Brown. A brief account of microscopical observations made in the months of June, July and August, 1827, on the particles contained in the pollen of plants; and on the general existence of active molecules in organic and inorganic bodies. Phil. Mag. 4 (1828) p.161.
[11] C. Canuto, M.Y. Hussaini, A. Quarteroni and T.A. Zang T.A. *Spectral Methods. Fundamentals in Single Domains*. Springer-Verlag, Berlin, 2006.
[12] J.W. Cahn, J.E. Hilliard. Free energy of a nonuniform system I. J. Chem. Phys. 28 (1958) p.258.
[13] J.W. Cahn. Free energy of a nonuniform system II. Thermodynamic basis. J. Chem. Phys. 30 (1959) p.1121.
[14] J.W. Cahn, J.E. Hilliard. Free energy of a nonuniform system III. J. Chem. Phys. 31 (1959) p.688.
[15] J.W. Cahn. On spinodal decomposition. Acta Metall. 9 (1961) p.795.
[16] J.W. Cahn and J.E. Hilliard. Spinodal Decomposition: A Reprise. Acta Metall. Mater. 19 (1971) p.151.
[17] S. Conti, B. Niethammer and Felix Otto. Coarsening rates in off-critical mixtures. SIAM J. Math. Anal. 37(6) (2006) p.1732. (electronic)
[18] H.E. Cook and J.E. Hilliard. Effect of Gradient Energy on Diffusion in Gold-Silver Alloys. J. Appl. Phys. 40(5) (1968) p.2191.
[19] H.E. Cook. Brownian motion in spinodal decomposition. Acta Metall. 18(3) (1970) p.297.
[20] H.E. Cook. Continuous Transformations. Materials Science and Engineering. 25 (1976) p.127.
[21] J. Cottrell, T. Hughes and Y. Bazilevs: Isogeometric Analysis: Toward Integration of CAD and FEA. Wiley (2009).
[22] M. Clausel. *Gaussian fields satisfying simultaneous operator scaling relations*. Recent developments in Fractals and related Fields: Applied and Numerical Harmonic Analysis, Part 4 (2010) p.327.
[23] D.L. Decker, J.D. Weiss and H.B. Vanfleet. Diffusion of Sn in Pb to 30 kbar. Phys. Rev. B. 16(6) (1977) p.2392.
[24] W. Dreyer and W.H. Müller. A study of the coarsening in tin/lead solders. Int. J. Solids Struct. 37(28) (2000) p.3841.
[25] W. Dreyer and W.H. Müller. Modelling diffusional coarsening in eutectic tin/lead solders: a quantitative approach. Int. J. Solids Struct. 38 (2001) p.1433.
[26] A. Einstein. *Über die von der molekularkinetischen Theorie der Wärme geforderte Bewegung von in ruhenden Flüssigkeiten suspendierten Teilchen*. Annalen der Physik 17 (1905) p.549. (german)
[27] A. Einstein. *Investigations on the Theory of Brownian Movement*. New York: Dover, 1956.
[28] K.R. Elder, T.M. Rogers and R.C. Desai. Early stages of spinodal decomposition for the Cahn-Hilliard-Cook model of phase separation. Phys. Rev. B. 38(7) (1988) p.4725.
[29] P. J. Flory. Thermodynamics of high polymer solutions. J. Chem. Phys. 10 (1942) p.51.
[30] H. Garcke, M. Rumpf and U. Weikard. The Cahn-Hilliard equation with elasticity: Finite element approximation and qualitative studies. Interfaces and Free Boundaries. 3 (2001) p.101.
[31] D. Gottlieb and S. Orzag. Numerical Analysis of Spectral Methods: Theory and Applications. SIAM, Philadelphia (1977).
[32] H. Gomez, V. M. Calo, Y. Bazilevs and T. J. R. Hughes. Isogeometric analysis of the Cahn-Hilliard phase-field model. Comput. Methods Appl. Mech. Engrg. 197 (2008) p.4333.
[33] D. Gupta, K. Vieregge and W. Gust. Interface diffusion in eutectic Sn-Pb solder. Acta mater. 47(1) (1999) p.5.
[34] K.A. Hawick. *Numerical Simulation and Role of Noise in the Cahn-Hilliard-Cook Equation below the Critical Dimension*. to appear in Proc. IASTED International Conference on Modeling, Identification and Control (MIC), 24-26 Nov. 2010, in Phuket, Thailand.
[35] K.A. Hawick and D.P. Playne. *Modelling and Visualizing the Cahn-Hilliard-Cook equation*. In: Proceedings of 2008 International Conference on Modeling, Simulation and Visualization Methods (MSV08), 2008, Las Vegas, Nevada.
[36] M. L. Huggins. Theory of solutions of high polymers. J. Am. Chem. Soc. 64 (1942) p.1712.
[37] D.A. Huse. Corrections to late-stage behavior in spinodal decomposition: Lifshitz- Slyozov scaling and Monte Carlo simulations. Physical Review B 34 (1986) p.7845.
[38] E.L. Huston, J.W. Cahn and J.E. Hilliard. Spinodal decomposition during continuous cooling. Acta Metall. 14(9) (1966) p.1053.
[39] M.A. Krivoglaz. *Theory of X-ray and Thermal Neutron Scattering by Real Crystals*. Plenum Press, New York, 1969.
[40] T. Küpper and N. Masbaum. Simulation of particle growth and Ostwald ripening via the Cahn-Hilliard equation. Acta Metall. Mater. 42(6) (1994) p.1847.
[41] P. Langevin. On the Theory of Brownian Motion. C. R. Acad. Sci. 146 (1908) p.530.
[42] L.D. Landau and E.M. Lifshitz. *Course of Theoretical Physics*. Volume 5, Statistical Physics, Chapter XII, Elsevier, 2009.
[43] I.M. Lifshitz and V.V. Slyozov. The kinetics of precipitation from supersaturated solid solution. Journal of Physical Chemistry Solids 19 (1961) p.35.
[44] N. Moelans, B. Blanpain and P. Wollants. An introduction to phase-field modeling of microstructure evolution. CALPHAD – Computer Coupling of Phase Diagrams and Thermochemistry. 32 (2008) p.268.
[45] A. Novick-Cohen and A. Shishkov. Upper bounds for coarsening for the degenerate Cahn-Hilliard equation. DCDS-A, 25 (2009) p.251.
[46] K.B. Rundmann and J.E. Hilliard. Early stages of spinodal decomposition in an aluminum-zinc alloy. Acta Metall. 15(6) (1967) p.1025.

[47] R.L.J.M. Ubachs, P.J.G. Schreurs, and M.G.D. Geers. A nonlocal diffuse interface model for microstructure evolution in tin-lead solder. J Mech Phys Solids. 52 (2004) p.1763.
[48] G. E. Uhlenbeck and L. S. Ornstein: On the theory of Brownian Motion. Physical Review. 36 (1930) p.823.
[49] C. Wagner. Theorie der Alterung von Niederschlägen durch Umlösen (Ostwald- Reifung). Zeitschrift für Elektrochemie 65 (1961) p.581.
[50] Y. Zhang, D.A. Benson, M.M. Meerschaert, E.M. LaBolle and H.P. Scheffler. Random walk approximation of fractional-order multiscaling anomalous diffusion. Phys. Rev. E 74 (2006) p.10.
[51] O. C. Zienkiewicz and R. L. Taylor. *The Finite Element Method. Vol. 1–3.* McGraw–Hill Book Company, 2003.